

See discussions, stats, and author profiles for this publication at: <https://www.researchgate.net/publication/235002976>

Structural Topology and Activation of an Initial Adenylate Kinase-Substrate Complex

ARTICLE in BIOCHEMISTRY · JANUARY 2013

Impact Factor: 3.02 · DOI: 10.1021/bi301460k · Source: PubMed

CITATIONS

5

READS

55

5 AUTHORS, INCLUDING:



Felix Christoph Weise

19 PUBLICATIONS 358 CITATIONS

SEE PROFILE



Kristoffer Brännström

Umeå University

29 PUBLICATIONS 350 CITATIONS

SEE PROFILE



Anders Olofsson

Umeå University

53 PUBLICATIONS 1,377 CITATIONS

SEE PROFILE

Structural Topology and Activation of an Initial Adenylate Kinase–Substrate Complex

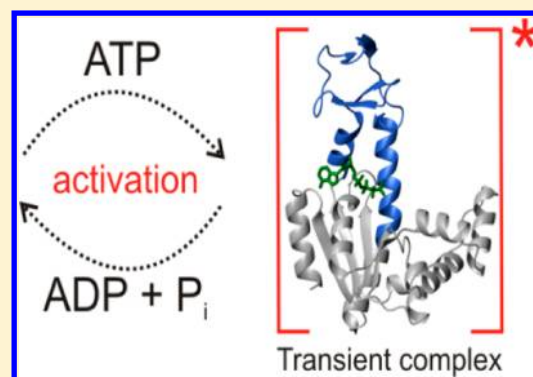
Jörgen Ådén,[†] Christoph F. Weise,[†] Kristoffer Brännström,[‡] Anders Olofsson,[‡] and Magnus Wolf-Watz^{*,†}

[†]Department of Chemistry, Chemical Biological Center, Umeå University, SE-901 87 Umeå, Sweden

[‡]Department of Medical Biochemistry and Biophysics, Chemical Biological Center, Umeå University, SE-901 87 Umeå, Sweden

S Supporting Information

ABSTRACT: Enzymatic activity is ultimately defined by the structure, chemistry, and dynamics of the Michaelis complex. A large number of experimentally determined structures between enzymes and substrates, substrate analogues, or inhibitors exist. However, transient, short-lived encounter and equilibrium structures also play fundamental roles during enzymatic reaction cycles. Such structures are inherently difficult to study with conventional experimental techniques. The enzyme adenylate kinase undergoes major conformational rearrangements in response to binding of its substrates, ATP and AMP. ATP is sandwiched between two binding surfaces in the closed and active enzyme conformation. Thus, adenylate kinase harbors two spatially distant surfaces in the substrate free open conformation, of which one is responsible for the initial interaction with ATP. Here, we have performed primarily nuclear magnetic resonance experiments on *Escherichia coli* adenylate kinase (AK_{eco}) variants that allowed identification of the site responsible for the initial ATP interaction. This allowed a characterization of the structural topology of an initial equilibrium complex between AK_{eco} and ATP. On the basis of the results, we suggest that the ATP binding mechanism for AK_{eco} is a mixture between “induced fit” and “conformational selection” models. It is shown that ATP is activated in the initial enzyme-bound complex because it displays an appreciable rate of nonproductive ATP hydrolysis. In summary, our results provide novel structural and functional insights into adenylate kinase catalysis.



One of the fundamental requirements for the viability of cellular organisms is that cellular chemical reactions occur on a time scale that is much faster than the turnover rate of global processes (such as cell division). These requirements are accomplished by the action of enzymes. With a simplistic view, enzymatic catalysis can be deconvoluted into well-defined microscopic steps, including (i) substrate binding, (ii) formation of a Michaelis complex (through, for instance, conformational rearrangements), (iii) chemical modification of a substrate into a product, and (iv) breakdown of the Michaelis complex and product release.¹ Any of the individual steps can be the rate-limiting step for catalysis, and the microscopic rate constants are defined by the activation barrier associated with each step. Understanding the functional coupling between enzyme dynamics for catalysis has attracted substantial interest over the past 10 years. In several cases [dihydrofolate reductase,² RNase A,³ cyclophilin A,⁴ and adenylate kinase (AK)⁵], it has been observed that catalysis is rate-limited by slow micro- to millisecond conformational rearrangements. The enzymes described above display “pre-existing equilibria” where the substrate free enzymes transiently populate “substrate-bound-like” structures. For AK isolated from *Escherichia coli* (AK_{eco}), it has been shown that the magnitude of the preexisting equilibrium influences the catalytic parameters k_{cat} and K_{M} .⁶ AK catalyzes the reversible interconversion of ATP

and AMP into two ADP molecules and is essential for the energy balance in the cell. The phosphotransfer reaction occurs with an associative mechanism.⁷ AK is a modular enzyme and contains distinct subdomains that are responsible for the binding to ATP and AMP; these subdomains are termed ATP_{lid} and AMP_{bd}, respectively (Figure 1). The CORE subdomain is dictating the global stability of the enzyme.^{8,9} We have shown that ATP binds to AK_{eco} (step i) with a highly dynamic mechanism. In the presence of saturating ATP concentrations, ATP_{lid} is interconverting between fully open and closed conformations.¹⁰ Interestingly, the statistical weights of the two states are almost equal, and this dynamic interconversion contrasts the common view of enzyme–substrate complexes as static low-entropy entities. Previous studies of step ii (above) have shown that the large scale conformational change in response to ATP binding occurs with an “order–disorder–order”¹¹ or “cracking”¹² mechanism. Even though detailed knowledge is available for many of the important steps during AK_{eco} catalysis, no direct structural information about the initial AK_{eco}–ATP complex has been published. Such complexes are inherently difficult to study

Received: October 27, 2012

Revised: January 10, 2013

Published: January 22, 2013

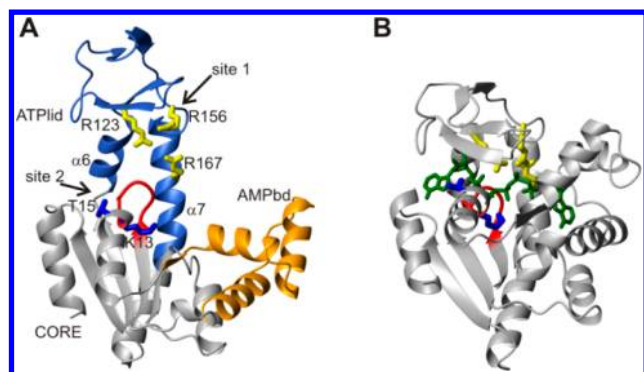


Figure 1. ATP interacting residues in AK_{eco} . Residues that make direct contacts with ATP are shown on open¹⁶ (A) and closed¹³ (B) AK_{eco} structures. ATP interacting residues in ATPlid and CORE are colored yellow and blue, respectively. ATPlid and AMPbd are colored blue and orange, respectively. The p-loop motif is colored red (note that K13 is part of the p-loop motif). The tight binding inhibitor Ap5A¹⁷ is colored green in panel B.

experimentally because they exist only transiently during reaction cycles. Nevertheless, these complexes are crucial for function, and knowledge of their structures will advance the general understanding of enzymatic catalysis. AK_{eco} interacts with ATP through two distinct binding surfaces, and ATP is sandwiched between residues in the ATPlid and CORE subdomains (Figure 1) in the fully closed state.¹³ Thus, AK_{eco} harbors two distinct ATP binding surfaces, both of which contribute to the complete binding free energy for ATP. At the microscopic level, AK_{eco} first interacts with ATP at either of the two surfaces forming an initial equilibrium complex. Following this initial binding event, a large conformational change occurs such that both surfaces engage in protein–ATP interactions. Here, we provide experimental observations that together conspire to define the structural topology of the initial AK_{eco} –ATP complex. As a consequence of the structural model, the mechanism for binding of ATP to AK_{eco} appears to be a hybrid between the classical induced fit¹⁴ and conformational selection models.¹⁵ It was also found that ATP is activated in the initial complex because it displays an appreciable rate of ATP hydrolysis.

MATERIALS AND METHODS

Protein Expression and Purification. Wild-type adenylate kinase and mutated variants were purified as described previously.⁵ Protein concentrations were determined by the absorption at 280 nm, using an extinction coefficient of 10430 $M^{-1} cm^{-1}$. Mutations were created by site-directed mutagenesis, using the Quickchange (Stratagene) approach. Primers were purchased from Eurofins MWG Operon, and mutations were confirmed via DNA sequencing (Eurofins MWG Operon). The genes encoding His-tagged AK_{eco} were ordered from GeneArt (Invitrogen) and inserted into a pET-3a expression vector. The AK_{p-loop} DNA sequence was synthesized as an artificial DNA sequence (Geneart) and subsequently subcloned into the pET-3a expression vector.

His-tagged protein for surface plasmon resonance experiments was expressed in LB medium and grown at 37 °C until OD_{600} reached 0.6, induced with IPTG (final concentration of 0.5 mM), and further grown overnight. The cells were resuspended in 50 mM Tris (pH 7.5), centrifuged at 5000 rpm for 30 min, and stored at –20 °C until they underwent

further purification. Purification was initiated by sonication, followed by centrifugation at 15000 rpm for 30 min. The protein pellet was resuspended in 50 mM Tris and 4 M GnaHCl (pH 7.5) and centrifuged at 15000 rpm for 30 min. The supernatant fraction was refolded overnight by dialysis against native buffer [50 mM Tris (pH 7.5)], supplemented with 0.03% 2-mercaptoethanol. After centrifugation at 15000 rpm for 30 min, the solution was filtered and imidazole and NaCl were added to final concentrations of 10 and 50 mM, respectively. Purification was accomplished on an IMAC column (Ni sepharose 6 Fast Flow, GE Healthcare) equilibrated with 50 mM Tris, 50 mM NaCl, and 10 mM imidazole (pH 7.5). The elution buffer was the same but included 500 mM imidazole. Selected fractions were further purified on a size exclusion column (Sephacryl S-100 HiPrep 26/60, GE Healthcare) equilibrated with 30 mM MES and 50 mM NaCl (pH 6.0), and protein purity was verified with sodium dodecyl sulfate–polyacrylamide gel electrophoresis.

Nuclear Magnetic Resonance (NMR) Spectroscopy.

Protein NMR experiments were conducted on a Bruker DRX 600 MHz spectrometer equipped with a 5 mm triple-resonance z-gradient cryoprobe. The NMR sample buffer consisted of 30 mM MES and 50 mM NaCl (pH 6.0) with 10% (volume/volume) 2H_2O . Sample concentrations varied between 400 and 800 μM . The temperature in all NMR experiments was 20 °C, which was calibrated prior to the experiments with a temperature probe inserted in the sample compartment of the cryoprobe. Assignments of 1H – ^{15}N HSQC spectra were made via three-dimensional ^{15}N NOESY-HSQC experiments using a pulse sequence from the Bruker library. NMR spectra were processed with NMRPipe¹⁸ and visualized in Ansig for Windows.¹⁹ Apparent ATP binding affinities (K_d^{app}) were quantified from chemical shifts and fits to a one-site binding model.¹⁰ Binding of ATP to all AK_{eco} variants is fast on the chemical shift time scale. Global K_d^{app} values were calculated as averages over residue specific affinities. Errors in the global fits were calculated from the standard deviation of the individual binding curves. ^{31}P NMR spectra were recorded at 20 °C on a 500 MHz Bruker DRX instrument equipped with a 5 mm broadband TBI probe. Acquisition parameters include a spectral width of 10 kHz, 8K points, 512 transients per FID, and a relaxation delay of 2 s. Spectra were processed in Topspin 2.0 (Bruker) and baseline-corrected and integrated using scripts written in Matlab 6.5. Chemical shifts were referenced to phosphoric acid.

Surface Plasmon Resonance (SPR) Analysis. Surface plasmon resonance binding experiments were performed at 25 °C on a Biacore 3000 instrument (GE Healthcare) and the results analyzed with Scrubber 2 (BioLogic Software). The nitrilotriacetic acid (NTA) sensor chip (GE or Xantec) was subjected to 100 mM $NiCl_2$ in HBS buffer without EDTA at a rate of 20 $\mu L/min$ for 5 min to obtain a metal chelating sensor surface. After NHS/EDC activation of the chip, the protein was injected at a rate of 5 $\mu L/min$ until the desired protein density was reached. Thereafter, the chip was blocked with ethanolamine. In all experiments, a reference surface that had been activated and subsequently blocked was used. As an additional reference, injection of buffers for double referencing was used in all experiments. The buffer for the experiments consisted of 100 mM Tris and 80 mM KCl with 2 mM $MgCl_2$ (pH 7.5). The concentration interval for Ap5A in these experiments varied between 15.6 nM and 2 μM .

RESULTS AND DISCUSSION

Here, we have performed experiments aimed to understand which of the two ATP interacting surfaces is responsible for the initial interaction between AK_{eco} and ATP. The first surface (site 1) include arginines 123, 156, and 167 (ATPlid), and the second surface (site 2) includes the p-loop motif together with threonine 15 in the CORE subdomain (Figure 1). The p-loop, or Walker A motif, is a conserved ATP binding sequence present in many proteins with ATPase activity.²⁰ The spatial separation of the ATP binding site into two distinct surfaces is favorable in terms of probing the structure of the initial ATP-bound complex. To experimentally identify the binding surface responsible for the initial ATP interaction, a set of AK_{eco} mutants in which the two binding sites were independently removed via replacement of key residues with alanine were made. A schematic illustration of the AK_{eco} variants analyzed in this study is provided in Figure 2.

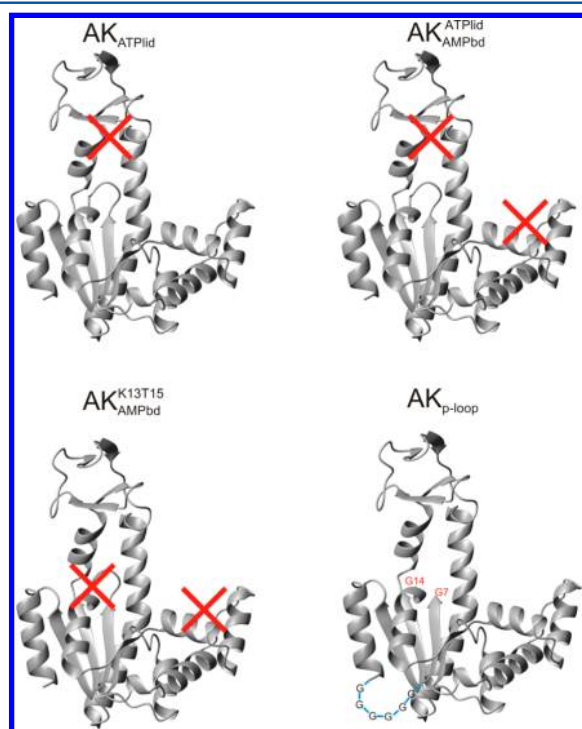


Figure 2. Mutational strategy used to identify the surface responsible for the initial interaction between AK_{eco} and ATP. The name of each mutant is printed above the corresponding image. The red crosses indicate the binding site(s) that has been removed by mutation.

Analysis of apparent ATP binding constants (K_d^{app}) and chemical shift perturbations in the mutated variants was used to identify the surface responsible for the initial ATP interaction. All mutants discussed here are well-folded proteins based on ¹H–¹⁵N heteronuclear single-quantum coherence (HSQC) NMR spectra. Both K_d^{app} values (Table 1) and chemical shift perturbations (Figure 3) have previously been quantified for wild-type (WT) AK_{eco}¹⁰ and used as a reference in this study. The ATP-induced chemical shift perturbations in AK_{eco} are distributed over a large part of the enzyme; these changes reflect (i) residues that are close to ATP and (ii) residues that undergo conformational changes in response to ATP binding.

Simultaneous mutation of arginines 123, 156, and 167 into alanine (mutant denoted AK_{ATPlid}) results in a protein in which

Table 1. Apparent Dissociation Constants (K_d^{app}) for Binding of ATP to ATPlid in AK_{eco} Variants Determined via NMR Spectroscopy

protein	K_d^{app} (μM)
wild-type	50 ± 31
AK _{ATPlid}	980 ± 130
AK _{ATPlid} AMPbd	1400 ± 230
AK _{K13T15} AMPbd	2100 ± 130

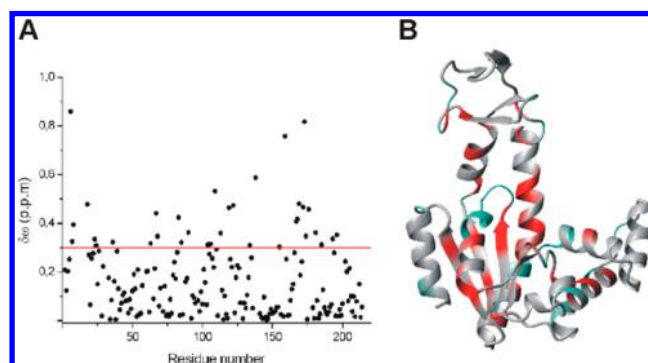


Figure 3. Structural response to ATP binding for WT AK_{eco}. (A) Compounded ¹⁵N and ¹H chemical shift perturbations resulting from ATP binding are calculated according to the equation $\delta\omega = 0.2|\Delta^{15}\text{N}| + |\Delta^1\text{H}|$ (parts per million), adapted from ref 10. The red line indicates the threshold value used in panel B. (B) Residues with a compounded chemical shift difference of >0.3 ppm (red line in panel A) in response to ATP binding are colored red on the open AK_{eco} structure. Unassigned and proline residues are colored turquoise.

ATP interaction site 1 is removed and the binding capacity of site 2 can be explored. The chemical shift perturbations in response to ATP binding in this AK_{eco} variant are localized to the p-loop and a few residues in its vicinity and also to AMPbd (Figure 4). Apparently, ATP can bind to site 2 in the mutant,

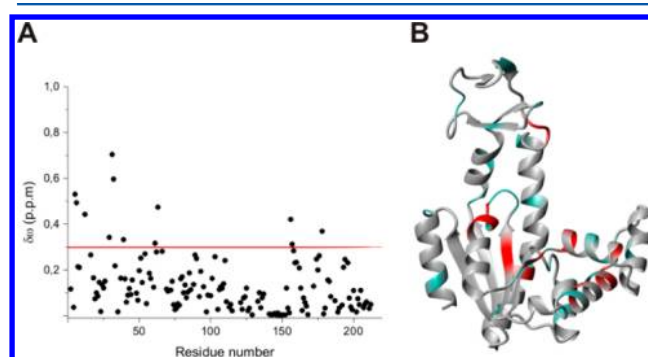


Figure 4. Structural response of AK_{ATPlid} to ATP binding. (A) Compounded ¹⁵N and ¹H chemical shift perturbations resulting from ATP binding. (B) Residues with a combined chemical shift difference of >0.3 ppm (red line in panel A) in response to ATP binding are colored red on the open AK_{eco} structure. Unassigned and proline residues are colored turquoise.

but with a substantially more narrow spatial distribution of chemical shift perturbations compared to that in the wild type. This result indicates that a large fraction of the chemical shift perturbations in the wild type are dependent on the conformational rearrangement. The K_d^{app} values for binding of ATP to the ATP and AMP binding sites in this variant are 980 and 960 μM, respectively. It is known that AMP can bind

nonspecifically to the ATP binding site,^{10,21} and this effect explains the AMP inhibition that occurs at AMP concentrations exceeding $\sim 200 \mu\text{M}$.²¹ No evidence of ATP inhibition of AK_{eco} exists, likely because ATP binds to AK_{eco} with a dissociation constant of $50 \mu\text{M}$ ¹⁰ and the conformational change subsequent to ATP binding sterically prohibits access of ATP to the AMP site. In the $\text{AK}_{\text{ATPlid}}$ mutant, the affinity for ATP is significantly reduced compared to that of the WT enzyme, and the enzyme cannot, because of the mutations, wrap around ATP. In this context, ATP can gain access to the AMP site, resulting in observable chemical shift perturbations.

To probe if the chemical shift perturbations in AMPbd in the $\text{AK}_{\text{ATPlid}}$ variant are due to nonspecific binding of ATP, we created the $\text{AK}_{\text{ATPlid}}$ mutant on the background of an AK_{eco} variant that is unable to bind AMP at the AMP binding site (simultaneous mutation of V39, A49, and M53 into glycine⁹). The resulting mutant is denoted $\text{AK}_{\text{AMPbd}}^{\text{ATPlid}}$. This variant does not bind ATP at the AMP site as evidenced by chemical shift perturbations (Figure 5), thus reinforcing the fact that ATP

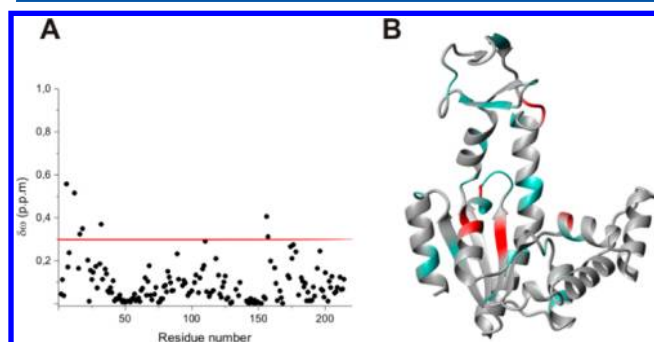


Figure 5. Structural response of $\text{AK}_{\text{AMPbd}}^{\text{ATPlid}}$ to ATP binding. (A) Compounded ^{15}N and ^1H chemical shift perturbations resulting from ATP binding. (B) Residues with a combined chemical shift difference of >0.3 ppm (red line in panel A) in response to ATP binding are colored red on the open AK_{eco} structure. Unassigned and proline residues are colored turquoise.

indeed binds nonspecifically to AMPbd in the $\text{AK}_{\text{ATPlid}}$ variant. Taken together, the results from the $\text{AK}_{\text{ATPlid}}$ and $\text{AK}_{\text{AMPbd}}^{\text{ATPlid}}$ variants provide two new insights. (i) Site 2 (i.e., p-loop sequence) is likely responsible for the initial ATP– AK_{eco} interaction, and (ii) ATP binds to the AMP site with a dissociation constant of ~ 1 mM. The latter interaction is, however, not observed in the WT enzyme because of steric hindrance and large difference in $K_{\text{d}}^{\text{app}}$ values for binding of ATP to the ATP and AMP sites.

If site 2 is solely responsible for the initial ATP– AK_{eco} complex, then it follows that upon disruption of site 2 no significant chemical shift perturbations should be observed in ATPlid (site 1). To test this prediction, we created an AK_{eco} variant in which K13 and T15 were replaced with alanine. This mutant was created on the background of the AK_{AMPbd} mutant to prevent binding of ATP to the AMP site. This variant is denoted $\text{AK}_{\text{AMPbd}}^{\text{K13T15}}$. We found that the $\text{AK}_{\text{AMPbd}}^{\text{K13T15}}$ mutant does not show any chemical shift perturbations in ATPlid at saturating ATP concentrations. There is, however, a weak residual interaction with the p-loop sequence (Figure 6). This is somewhat surprising because two important side chain interactions with ATP are removed. Mutation of K13 into alanine in muscle AK results in an $\sim 10^4$ -fold decrease in k_{cat} and a 5-fold increase in K_{M} .²² Apparently, the p-loop sequence

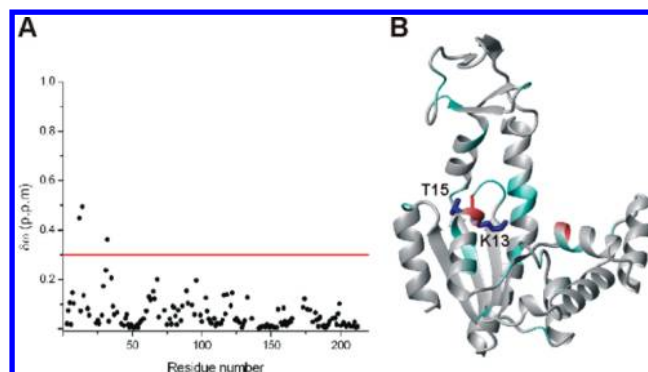


Figure 6. Structural response of $\text{AK}_{\text{AMPbd}}^{\text{K13T15}}$ to ATP binding. (A) Compounded ^{15}N and ^1H chemical shift perturbations resulting from ATP binding. The red line indicates the threshold value used in panel B. (B) Residues with a combined chemical shift difference of >0.3 ppm in response to ATP binding are colored red on the open AK_{eco} structure. Unassigned and proline residues are colored turquoise.

displays weak ATP binding affinity even when K13 and T15 are replaced with alanine. To completely remove the interaction of ATP with site 2, it is thus necessary to remove the p-loop segment altogether.

To accomplish this goal, we made a circular permutation of the AK_{eco} sequence such that residues 14 and 7 become the new N- and C-termini, respectively. The sequence is closed by introducing a six-glycine linker between the original C- and N-termini. This mutant is denoted $\text{AK}_{\text{p-loop}}$ and is illustrated schematically in Figure 2. In the permuted AK_{eco} variant, the p-loop is removed, and in addition, a positive charge and a negative charge are introduced at the new N- and C-termini, respectively. $\text{AK}_{\text{p-loop}}$ is a folded protein based on a high-quality and well-dispersed ^1H – ^{15}N HSQC spectrum (Figure S1 of the Supporting Information). The stability of this mutant is, however, compromised compared to that of the wild type as the protein precipitated when it was incubated at $>20^\circ\text{C}$. As a comparison, the melting point of the wild-type enzyme is 57°C .¹¹ Even though only partial assignments could be obtained for apo- $\text{AK}_{\text{p-loop}}$, it is evident that removal of the p-loop sequence completely eliminated binding of ATP to both binding sites 1 and 2 (Figure 7). This result reinforces the fact that site 2 harbors the initial ATP binding activity in AK_{eco} . With the ATP binding activity removed at the catalytically relevant binding site, ATP instead binds to the AMP binding site with an affinity of $750 \mu\text{M}$ in analogy to that of the $\text{AK}_{\text{ATPlid}}$ variant. With identification of site 2 as the initial ATP-interacting epitope, a model of the structural topology of the initial AK_{eco} –ATP complex can be generated (Figure 8). The model is by definition oversimplified because ATPlid interconverts between open and closed states in the presence of ATP in the wild-type enzyme.¹⁰ Nevertheless, the model captures the basic features of the initial ATP– AK_{eco} complex.

ATP Activation in the Initial AK_{eco} Complex. To be efficient catalysts, enzymes must simultaneously accomplish several functionally orthogonal tasks. Substrates must be aligned perfectly to facilitate the chemical step; unwanted side reactions must be suppressed, and the substrates should be activated. For AK_{eco} , the substrates are arranged optimally for phosphotransfer chemistry.¹³ The distance between the attacking $\alpha\text{-O2}$ atom on AMP and the γ -phosphorus on ATP is $3\text{--}3.4 \text{ \AA}$.²⁴ Nonproductive hydrolysis of ATP into ADP and P_i by AK_{eco} can be observed via ^{31}P NMR by quantifying the

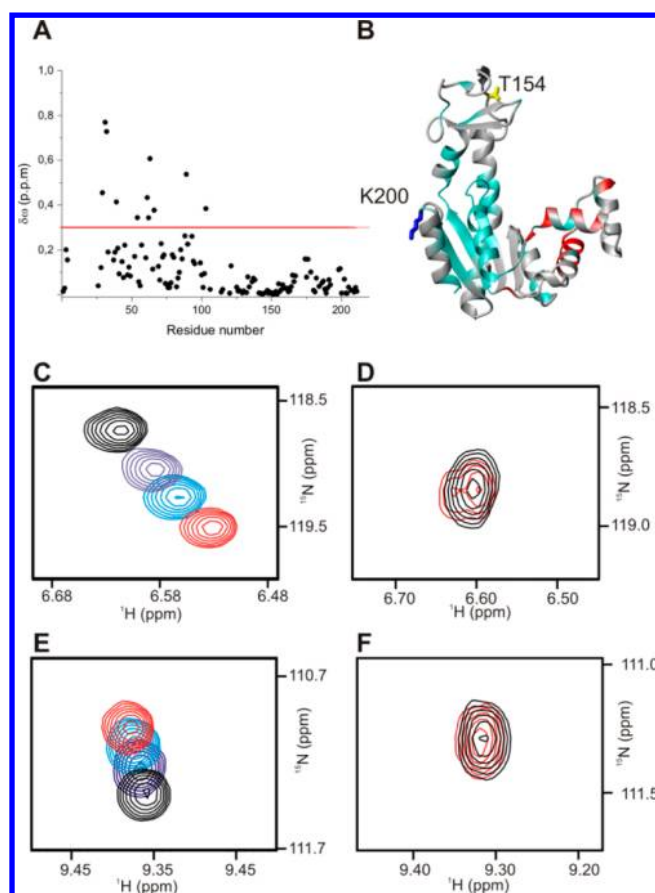


Figure 7. Structural response of AK_{p-loop} to ATP binding. (A) Compounded ^{15}N and 1H chemical shift perturbations resulting from ATP binding. (B) Residues with a combined chemical shift difference of >0.3 ppm (red line in panel A) in response to ATP binding are colored red on the open AK_{eco} structure. Unassigned and proline residues are colored turquoise. (C and D) Chemical shift perturbations for residue T154 (yellow in panel B) that is sensitive to ATP binding at site 1 in response to ATP binding for WT AK_{eco} (C) and AK_{p-loop} (D). (E and F) Chemical shift perturbations for residue K200 (blue in panel B) that is sensitive to ATP binding at site 2 in response to ATP binding for wild-type AK_{eco} (E) and AK_{p-loop} (F). The color coding in panels C–F is as follows: black for 0 mM ATP, purple for 0.2 mM ATP, blue for 0.4 mM ATP, and red for 10 mM ATP.

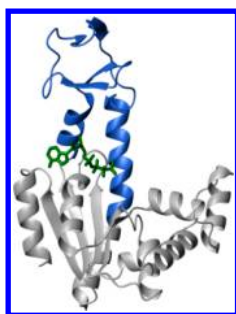


Figure 8. Structural topology of the initial equilibrium ATP- AK_{eco} complex. The model was created by superimposing substrate free open AK_{eco} onto that of yeast adenylate kinase in complex with the nonhydrolyzable ATP analogue AMPPCF $_2$ P.²³

intensity of the P_i peak as a function of time. For wild-type AK_{eco} , no buildup of P_i was observed for extensive periods of time (>16 h). Hence, this nonproductive side reaction is effectively suppressed by AK_{eco} . In contrast, in the case of

AK_{ATPld} , a P_i peak that gradually increased in intensity was observed. A reaction scheme that describes the nonproductive hydrolysis of ATP is shown below:



where $[AK:ATP]$ corresponds to a Michaelis complex of the reaction. To extract the k_{cat} value from quantified rates of hydrolysis, it is useful to set up the equation for the rate of P_i production.

$$\frac{dP_i}{dT} = k_{cat}[AK:ATP]$$

From this expression, it is evident that the k_{cat} value is obtained by scaling the rates of hydrolysis (dP_i/dT) by the concentration of the Michaelis complex. The concentration of the Michaelis complex is computed by using a K_d value of 1 mM (Table 1) and an initial ATP concentration of 20 mM. The ATP concentration is in large excess so the concentration of ATP and of the Michaelis complex can be treated as being constant over the experiment.

The experiment for AK_{ATPld} was performed at both 100 and 200 μM protein; both these concentrations gave very similar k_{cat} values ($5.0 \times 10^{-4} s^{-1}$) when scaled by the ES concentration (Figure 9). This corresponds to a 30000-fold rate enhancement compared to noncatalyzed hydrolysis of ATP at pH 6.0.²⁵

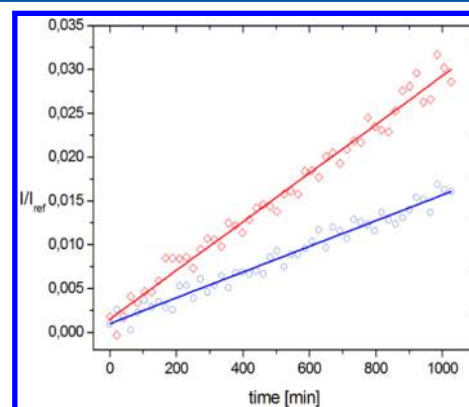


Figure 9. Phosphate buildup resulting from hydrolysis of ATP in the AK_{ATPld} mutant. Phosphate buildup was probed via ^{31}P NMR spectroscopy. The experimental conditions were 20 °C and 20 mM ATP. The blue and red symbols correspond to data from experiments with 100 and 200 μM AK_{ATPld} , respectively. The solid lines correspond to linear fits to the buildup of inorganic phosphate.

The analysis holds under conditions where K_M is equal to K_d , and these conditions are fulfilled when k_{off} is much larger than k_{cat} . The k_{off} rate constant for dissociation of ATP from AK_{ATPld} was estimated to be $1480 s^{-1}$. To derive this, we used the k_{on} rate constant for binding of Ap5A to AK_{eco} determined from surface plasmon resonance experiments (Figure S2 of the Supporting Information; $k_{on} = 1.48 \times 10^6 M^{-1} s^{-1}$) and a K_d of 1 mM for binding of ATP to the AK_{ATPld} variant (Table 1). Hence, the estimated k_{off} is much larger than k_{cat} , and as a consequence, K_M equals K_d . From these observations, we draw two conclusions. (1) ATP is activated already at the initial interaction with AK_{eco} (Figures 8 and 9), and (2) nonproductive ATP hydrolysis is effectively eliminated in wild-type

AK_{eco} because of dehydration of the active site in response to closure of ATPlid.¹³

CONCLUSIONS

The structural model presented here (Figure 8), together with the crystal structures of open¹⁶ and closed¹³ AK_{eco}, suggests that the ATP binding mechanism is a hybrid between “induced fit”¹⁴ and “conformational selection”¹⁵ models (Figure 10). The

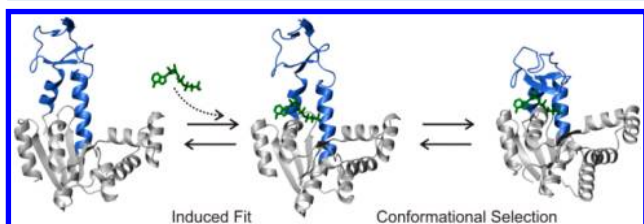


Figure 10. Hybrid ATP binding model for AK_{eco}. Substrate free AK_{eco} interacts with ATP using an induced fit mechanism to form the initial equilibrium complex. Closure of ATPlid on ATP bound to site 2 occurs with a conformational selection event that on the molecular level involves an order–disorder–order transition.¹¹ The structure of the closed AK_{eco}–ATP complex is that of yeast adenylate kinase in complex with the nonhydrolyzable ATP analogue AMPPCF₂P.²³

initial interaction with ATP at site 2 is accompanied with only modest structural perturbations of the p-loop sequence (Figure S3 of the Supporting Information). We classify this change as an induced fit rearrangement.¹⁴ The following thermally driven closure of ATPlid,^{11,26} with ATP bound to site 2, is classified as a “conformational selection (i.e., one site MWC model²⁷)” event. It should be noted that a pure conformational selection model is not feasible because a fully closed ATPlid sterically excludes penetration of ATP into the binding site. Preclusion of conformational selection due to solvent occlusion of an enzyme active site has previously been suggested for phosphoenolpyruvate carboxykinase.²⁸ A similar two-step binding mechanism has been suggested for iron uptake by duck ovotransferrin.²⁹ The structural characterization of the initial ATP–AK_{eco} complex resulting from our experiments will be important in simulations of the open–closed transition. For instance, in a recent simulation, it was assumed that the initial ATP interaction is mediated by the three arginines (site 1) in ATPlid (Figure 1).³⁰ It is important to note that the structural model presented here is that of an initial equilibrium complex between AK_{eco} and ATP. The first encounter between AK_{eco} and ATP in an encounter complex is not addressed in this analysis. Detailed descriptions of the structural ensembles of encounter complexes for protein–protein association do, however, exist. These ensembles were obtained from an extensive analysis of NMR paramagnetic relaxation enhancement.^{31,32} Our ³¹P NMR data show that wild-type AK_{eco} suppresses nonproductive water-mediated hydrolysis of ATP; hence, the conformational change during substrate binding effectively removes water molecules from the active site. In contrast, when the ATP binding reaction is arrested in the initial equilibrium complex, ATP is hydrolyzed into ADP and inorganic phosphate. This observation shows that ATP is activated already in the initial complex with AK_{eco}. Taken together, our results add new insights into adenylate kinase catalysis, and the methodology used to identify the initial ATP binding site may be also used for other protein–substrate complexes.

ASSOCIATED CONTENT

Supporting Information

¹H–¹⁵N HSQC spectrum of AK_{p-loop} (Figure S1), Ap5A binding kinetics with AK_{eco} obtained from surface plasmon resonance (Figure S2), and illustration of the induced fit movement of the p-loop segment upon binding of ATP to AK_{eco} (Figure S3). This material is available free of charge via the Internet at <http://pubs.acs.org>.

AUTHOR INFORMATION

Corresponding Author

*E-mail: magnus.wolf-watz@chem.umu.se. Telephone: +46-90-786 76 90. Fax: +46-90-786 76 55.

Funding

This work was supported by the Swedish Research Council (621-2010-5247 to M.W.-W. and 521-2011-2619 to Å.O.), the Kempe foundation (to M.W.-W. and Å.O.), and a Umeå University “Young Researcher award” to M.W.-W.

Notes

The authors declare no competing financial interest.

ACKNOWLEDGMENTS

We thank Gerhard Gröbner and Pernilla Wittung-Stafshede for valuable discussions during the course of this study.

REFERENCES

- (1) Fersht, A. (2000) *Structure and mechanism in protein science*, W. H. Freeman and Co., New York.
- (2) Boehr, D. D., McElheny, D., Dyson, H. J., and Wright, P. E. (2006) The dynamic energy landscape of dihydrofolate reductase catalysis. *Science* 313, 1638–1642.
- (3) Beach, H., Cole, R., Gill, M. L., and Loria, J. P. (2005) Conservation of mus-ms enzyme motions in the apo- and substrate-mimicked state. *J. Am. Chem. Soc.* 127, 9167–9176.
- (4) Eisenmesser, E. Z., Millet, O., Labeikovsky, W., Korzhnev, D. M., Wolf-Watz, M., Bosco, D. A., Skalicky, J. J., Kay, L. E., and Kern, D. (2005) Intrinsic dynamics of an enzyme underlies catalysis. *Nature* 438, 117–121.
- (5) Wolf-Watz, M., Thai, V., Henzler-Wildman, K., Hadjipavlou, G., Eisenmesser, E. Z., and Kern, D. (2004) Linkage between dynamics and catalysis in a thermophilic-mesophilic enzyme pair. *Nat. Struct. Mol. Biol.* 11, 945–949.
- (6) Ådén, J., Verma, A., Schug, A., and Wolf-Watz, M. (2012) Modulation of a Pre-existing Conformational Equilibrium Tunes Adenylate Kinase Activity. *J. Am. Chem. Soc.* 134, 16562–16570.
- (7) Abele, U., and Schulz, G. E. (1995) High-resolution structures of adenylate kinase from yeast ligated with inhibitor Ap5A, showing the pathway of phosphoryl transfer. *Protein Sci.* 4, 1262–1271.
- (8) Bae, E., and Phillips, G. N., Jr. (2006) Roles of static and dynamic domains in stability and catalysis of adenylate kinase. *Proc. Natl. Acad. Sci. U.S.A.* 103, 2132–2137.
- (9) Rundqvist, L., Ådén, J., Sparrman, T., Wallgren, M., Olsson, U., and Wolf-Watz, M. (2009) Noncooperative Folding of Subdomains in Adenylate Kinase. *Biochemistry* 48, 1911–1927.
- (10) Ådén, J., and Wolf-Watz, M. (2007) NMR identification of transient complexes critical to adenylate kinase catalysis. *J. Am. Chem. Soc.* 129, 14003–14012.
- (11) Olsson, U., and Wolf-Watz, M. (2010) Overlap between folding and functional energy landscapes for adenylate kinase conformational change. *Nat. Commun.* 1, 111.
- (12) Whitford, P. C., Miyashita, O., Levy, Y., and Onuchic, J. N. (2007) Conformational transitions of adenylate kinase: Switching by cracking. *J. Mol. Biol.* 366, 1661–1671.
- (13) Müller, C. W., and Schulz, G. E. (1992) Structure of the complex between adenylate kinase from *Escherichia coli* and the

inhibitor Ap5A refined at 1.9 Å resolution. A model for a catalytic transition state. *J. Mol. Biol.* 224, 159–177.

(14) Koshland, D. E. (1958) Application of a Theory of Enzyme Specificity to Protein Synthesis. *Proc. Natl. Acad. Sci. U.S.A.* 44, 98–104.

(15) Lange, O. F., Lakomek, N. A., Fares, C., Schroder, G. F., Walter, K. F., Becker, S., Meiler, J., Grubmüller, H., Griesinger, C., and de Groot, B. L. (2008) Recognition dynamics up to microseconds revealed from an RDC-derived ubiquitin ensemble in solution. *Science* 320, 1471–1475.

(16) Müller, C. W., Schlauderer, G. J., Reinstein, J., and Schulz, G. E. (1996) Adenylate kinase motions during catalysis: An energetic counterweight balancing substrate binding. *Structure* 4, 147–156.

(17) Lienhard, G. E., and Secemski, I. I. (1973) P1,P5-Di(adenosine-5')pentaphosphate, a potent multisubstrate inhibitor of adenylate kinase. *J. Biol. Chem.* 248, 1121–1123.

(18) Delaglio, F., Grzesiek, S., Vuister, G. W., Zhu, G., Pfeifer, J., and Bax, A. (1995) NMRPipe: A multidimensional spectral processing system based on UNIX pipes. *J. Biomol. NMR* 6, 277–293.

(19) Helgstrand, M., Kraulis, P., Allard, P., and Härd, T. (2000) Ansig for Windows: An interactive computer program for semi-automatic assignment of protein NMR spectra. *J. Biomol. NMR* 18, 329–336.

(20) Walker, J. E., Saraste, M., Runswick, M. J., and Gay, N. J. (1982) Distantly related sequences in the α - and β -subunits of ATP synthase, myosin, kinases and other ATP-requiring enzymes and a common nucleotide binding fold. *EMBO J.* 1, 945–951.

(21) Sinev, M. A., Sineva, E. V., Ittah, V., and Haas, E. (1996) Towards a mechanism of AMP-substrate inhibition in adenylate kinase from *Escherichia coli*. *FEBS Lett.* 397, 273–276.

(22) Byeon, L., Shi, Z., and Tsai, M. D. (1995) Mechanism of adenylate kinase. The “essential lysine” helps to orient the phosphates and the active site residues to proper conformations. *Biochemistry* 34, 3172–3182.

(23) Schlauderer, G. J., Proba, K., and Schulz, G. E. (1996) Structure of a mutant adenylate kinase ligated with an ATP-analogue showing domain closure over ATP. *J. Mol. Biol.* 256, 223–227.

(24) Berry, M. B., Meador, B., Bilderback, T., Liang, P., Glaser, M., and Phillips, G. N., Jr. (1994) The closed conformation of a highly flexible protein: The structure of *E. coli* adenylate kinase with bound AMP and AMPPNP. *Proteins* 19, 183–198.

(25) Stockbridge, R. B., and Wolfenden, R. (2009) The intrinsic reactivity of ATP and the catalytic proficiencies of kinases acting on glucose, N-acetylgalactosamine, and homoserine: A thermodynamic analysis. *J. Biol. Chem.* 284, 22747–22757.

(26) Henzler-Wildman, K. A., Thai, V., Lei, M., Ott, M., Wolf-Watz, M., Fenn, T., Pozharski, E., Wilson, M. A., Petsko, G. A., Karplus, M., Hübner, C. G., and Kern, D. (2007) Intrinsic motions along an enzymatic reaction trajectory. *Nature* 450, 838–844.

(27) Monod, J., Wyman, J., and Changeux, J. P. (1965) On the Nature of Allosteric Transitions: A Plausible Model. *J. Mol. Biol.* 12, 88–118.

(28) Sullivan, S. M., and Holyoak, T. (2008) Enzymes with lid-gated active sites must operate by an induced fit mechanism instead of conformational selection. *Proc. Natl. Acad. Sci. U.S.A.* 105, 13829–13834.

(29) Lindley, P. F., Bajaj, M., Evans, R. W., Garratt, R. C., Hasnain, S. S., Jhoti, H., Kuser, P., Neu, M., Patel, K., Sarra, R., Strange, R., and Walton, A. (1993) The mechanism of iron uptake by transferrins: The structure of an 18 kDa NII-domain fragment from duck ovotransferrin at 2.3 Å resolution. *Acta Crystallogr. D* 49, 292–304.

(30) Pislakov, A. V., Cao, J., Kamerlin, S. C., and Warshel, A. (2009) Enzyme millisecond conformational dynamics do not catalyze the chemical step. *Proc. Natl. Acad. Sci. U.S.A.* 106, 17359–17364.

(31) Tang, C., Iwahara, J., and Clore, G. M. (2006) Visualization of transient encounter complexes in protein-protein association. *Nature* 444, 383–386.

(32) Bashir, Q., Volkov, A. N., Ullmann, G. M., and Ubbink, M. (2010) Visualization of the encounter ensemble of the transient

electron transfer complex of cytochrome c and cytochrome c peroxidase. *J. Am. Chem. Soc.* 132, 241–247.